Eleventh International Conference on CFD in the Minerals and Process Industries
CSIRO, Melbourne, Australia
7-9 December 2015

EFFECT OF OPERATING PRESSURE ON PARTICLE TEMPERATURE DISTRIBUTION IN A FLUIDIZED BED WITH HEAT PRODUCTION

Zizi LI, Martin van Sint ANNALAND, J.A.M. (Hans) KUIPERS, Niels G. DEEN*

Multiphase Reactors Group, Department of Chemical Engineering & Chemistry,
Eindhoven University of Technology, P.O. Box 513, 5600 MB Eindhoven, The Netherlands
Dutch Polymer Institute (DPI), P.O. Box 902, 5600 AX Eindhoven, the Netherlands.

*Corresponding author, E-mail address: N.G.Deen@tue.nl, tel: +31 402473681

ABSTRACT

The effect of elevated pressure on gas-solid heat transfer in an olefin polymerization fluidized bed was numerically analysed by using an in-house developed 3-D computational fluid dynamics code coupled with a discrete element model (CFD-DEM). To mimic the heat production due to the polymerization reaction, a constant volumetric heat production was implemented in the particle energy equation. Instantaneous snapshots of the thermal driving force (the difference of single particle temperature and bed-average gas temperature) are shown to give an insight into the particle temperature distribution in the fluidized bed. Furthermore, it was found from the Probability Distribution Function (PDF) of the particle temperature that increasing the operating pressure the average particle temperature drops and the bed becomes more isothermal. Moreover, the average particle-gas heat transfer coefficient was found to increase with increasing operating pressure. From the spatial distribution of the instantaneous Nusselt number, it becomes apparent that the high heat transfer regions are found in the wake of rising bubbles, whereas low heat transfer rates are found in the clouds of the bubbles. The effective heat transfer coefficient for pressurized fluidized beds can be well characterized by means of the empirical Gunn's correlation, provided that it is based on the particle Reynolds number depending on the gas velocity and the bed porosity at the minimum fluidization condition.

NOMENCLATURE

C_p	Specific heat capacity of particle	J/kg/K
d_p	Particle diameter	m
d_{cell}	Length of grid cell	m
$\mathbf{g}$	Gravity	m/s^2
h	Effective interfacial heat transfer coefficient	W/m^2/K
k_g	Fluid thermal conductivity	W/m/K
k_g^{eff}	Effective thermal conductivity of the gas	W/m/K
$\mathbf{I}$	Unit tensor	-
m_a	Mass of individual particle	kg
N_p	Particle number in the bed	-
Nu_p	Particle Nusselt number	-
Pr	Prandtl number	-
Q_p	Source term for the interphase heat exchange	W/m^3
$\mathbf{q}$	Heat flux	W/m^2
$\dot{q}$	Volumetric heat production	W/m^3
$\mathbf{r}_a$	Particle position	m
Re_p	Particle Reynolds number	-
$\mathbf{S}$	Body force exerted by particle on fluid	kg·m/s^2
$\mathbf{T}_{contact,a}$	Particle torque	kg·m/s
t	Simulation time	s
T	Temperature	K
$T_{p,m}$	Particle melting point	K
$\boldsymbol{u_g}$	Gas velocity	m/s
u_0	Superficial velocity	m/s
$\boldsymbol{v_a}$	Particle velocity	m/s
V_a	Particle volume	m^3
x	x direction	m
y	y direction	m
z	z direction	m
ε	Volume fraction	
ρ	Density	kg/m3
τ	Newtonian stress tensor	N/m^2
μ	Dynamic viscosity of gas	kg/(m s)
σ	Standard deviation of particle temperature	K
β	Inter-phase momentum coefficient	kg/m^{3}s
$\boldsymbol{\Theta}$	Particle angular velocity	rad/s

INTRODUCTION

Fluidized bed reactors (FBR) operated at elevated pressure have been utilized to carry out a variety of industrial processes. For example, heterogeneous olefin polymerization benefits from operation at elevated pressure (up to 20 bar) which leads to a higher degree of chemical conversion. To optimize the highly exothermic olefin polymerization conducted in FBR, fundamental knowledge of the hydrodynamics and heat transfer performance as a function of the operating pressure is required. The influence of pressure on the bed hydrodynamics has been studied by utilizing several experimental methods, i.e. electrical capacitance tomography (ECT) and X-ray tomography (Sidorenko and Rhodes, 2004; Yates and Simons, 1994). It has been reported from experimental studies that hydrodynamic characteristics of fluidized beds strongly depend on the operating pressure, i.e. the minimum fluidization velocity, bubble formation, bubble size, evolution and trajectory, etc.

In the past decade, due to the ongoing development of computational technology, the effects of pressure on the hydrodynamics of FBR have been investigated more thoroughly by numerical methods. Li and Kuipers (2002) investigated the pressure effect with a CFD-DEM approach, where they found that an elevated pressure

could reduce the incipient fluidization velocity, while providing a wider operating window for uniform fluidization. It narrows down the bubbling regime and leads to a quick transition to the turbulent regime. They also observed that an elevated operating pressure suppresses bubble growth and therefore produces more uniform gas-solid flow structures. A number of fluidization features, such as the bubble behaviour, flow patterns, solids mixing and particle granular temperature have been investigated by Godlieb et al. (2008) with state-of-art CFD-DEM simulations. They reported that at elevated pressure, the gas-particle interaction is enhanced and becomes relatively more important as compared to the particle-particle interaction. The bubble size also decreases, whereas the bubble breakage rate increases. Solids mixing is also enhanced at elevated pressure condition. It is noticed that most of these studies describe the effect of elevated pressure on the hydrodynamics of fluidized bed, while very little has been done on the altered gas-particle heat transfer behaviour or the combination of these two aspects.

It is known that elevated pressures can enhance the wall-to-bed heat transfer in fluidized beds, however, there is a lack of detailed information of the pressure effect on gas-particle heat transport inside of the bed. Therefore, in this paper the effect of pressure on the heat transport in fluidized beds has been studied considering both the effects of the increased density and the effect of the altered hydrodynamics.

This work is organized as follows. First details of the governing equations of the CFD-DEM model are given. A constant heat source for mimicking the polypropylene polymerization reaction heat has been added to the particle model with an estimated value from literature (Choi and Ray, 1985). In the results and discussion section, the hydrodynamics is characterized on the basis of the time averaged probability distribution function (PDF) of the bed porosity. Then, the particle temperature PDF of mono-dispersed particles, instantaneous snapshots of the driving force, particle Reynolds number (Re_p) and particle Nusselt number (Nu_p) distribution are discussed and analysed to quantitatively describe the pressure effect on the convective gas-particle heat transfer in fluidized beds.

MODEL DESCRIPTION

Numerical Model and Solution Methodology

Gas phase model

In the CFD-DEM model, the gas phase is described by the continuity equation and the volume-averaged Navier-Stokes equations:

$$\frac{\partial(\varepsilon_g \rho_g)}{\partial t} + (\nabla \cdot \varepsilon_g \rho_g \mathbf{u}_g) = 0 \tag{1}$$

$$\frac{\partial(\varepsilon_g \rho_g \mathbf{u}_g)}{\partial t} + \nabla \cdot (\varepsilon_g \rho_g \mathbf{u}_g \mathbf{u}_g) = -\varepsilon_g \nabla p_g - \nabla \cdot (\varepsilon_g \boldsymbol{\tau}_g) + \varepsilon_g \rho_g \mathbf{g} - \mathbf{S} \tag{2}$$

where ε_g, ρ_g, and $\mathbf{u}_g$ are the volume fraction, density and the velocity vector of the gas phase, respectively. In this case the gas density is calculated from the equation of state for ideal gases. $\boldsymbol{\tau}_g$ is the gas phase viscous stress tensor, which is assumed to obey the general Newtonian form:

$$\boldsymbol{\tau}_g = -\boldsymbol{\mu}_g[(\nabla \mathbf{u}_g) + (\nabla \mathbf{u}_g)^{\mathrm{T}} - \frac{2}{3}(\nabla \cdot \mathbf{u}_g)\mathbf{I}] \tag{3}$$

μ_g and $\mathbf{I}$ are the gas phase viscosity and the unit tensor, respectively. $\mathbf{S}$ is the sink term that accounts for the momentum exchange between the gas and the particles:

$$\mathbf{S} = \sum_{\forall a \in V} \frac{V_a \beta}{1-\varepsilon_g}(\mathbf{u}_g - \mathbf{v}_a) D(\mathbf{r} - \mathbf{r}_a) \tag{4}$$

Here D is the distribution function, which is used to distribute the force exerted by the particles on the gas phase in an Eulerian grid cell with volume V. β is the inter-phase momentum exchange coefficient, which can be calculated using a closure equation for the dimensionless drag force (F_{drag}). In this work, the Ergun equation (Ergun 1952) has been used for the dense regime and the Wen and Yu drag equation (Wen and Yu, 1966) for the dilute regime:

$$F_{drag} = \frac{\beta d_p^2}{\mu} = \begin{cases} 150\dfrac{1-\varepsilon_g}{\varepsilon_g} + 1.75\varepsilon_g \,\mathrm{Re}_p & (if\ \varepsilon_g < 0.8) \\ \dfrac{3}{4} C_D \,\mathrm{Re}_p (1-\varepsilon_g)\varepsilon_g^{-2.65} & (if\ \varepsilon_g > 0.8) \end{cases} \tag{5}$$

with:

$$\mathrm{Re}_p = \frac{\varepsilon_p \rho_p \left|\mathbf{u}_g - \mathbf{v}_p\right| d_p}{\mu_g} \tag{6}$$

and

$$C_d = \frac{24}{\mathrm{Re}_p}(1 + 0.15\mathrm{Re}_p^{\,0.687}) \tag{7}$$

The thermal energy equation for the gas phase is given by:

$$C_{p,\mathrm{g}}\left[\frac{\partial(\varepsilon_g \rho_g T_g)}{\partial t} + (\nabla \cdot \varepsilon_g \rho_g \mathbf{u}_g T_g)\right] = -(\nabla \cdot \varepsilon_g \mathbf{q}) + Q_p \tag{8}$$

where Q_p represents the source term originating from the interphase energy transport whereas $\mathbf{q}$ is the heat flux due to heat conduction and given by Fourier's law:

$$\mathbf{q} = -k_g^{eff} \nabla T_g \tag{9}$$

where k_g^{eff} is the effective thermal conductivity of the gas phase, which can be expressed in terms of the fluid thermal conductivity (k_{g}):

$$k_g^{eff} = \frac{1-\sqrt{1-\varepsilon_g}}{\varepsilon_g} k_g \tag{10}$$

The source term Q_p is given by:

$$Q_p = \frac{1}{V}\sum_{\forall a \in V} hA_{p,a}(T_{p,a} - T_g) D(\mathbf{r} - \mathbf{r}_{p,a}) \tag{11}$$

where T_{g} is the temperature of the gas phase at whereas $T_{\mathrm{p,a}}$ is the temperature of particle a.

Discrete particle model

The particles are individually tracked by solving Newton's second law of motion for both translational and rotational motion:

$$m_a \frac{\mathrm{d}^2 \mathbf{r}_a}{\mathrm{d}t^2} = -V_a \nabla p + \frac{\beta V_a}{1-\varepsilon_g}(\mathbf{u}-\mathbf{v}_a) + m_a \mathbf{g} + \sum_{a \neq b} \mathbf{F}_{contact,a} \quad (12)$$

$$I_a \frac{\mathrm{d}^2 \boldsymbol{\Theta}_a}{\mathrm{d}t^2} = \mathbf{T}_{contact,a} \quad (13)$$

Here, $\mathbf{r}_a$ is the position of particle 'a'. The translational motion of each particle is caused by the pressure gradient, drag force, gravity, and contact forces due to collisions with other particles and the confining walls. The rotational motion of the particles is taken into consideration by means of the angular displacement $\boldsymbol{\Theta}_a$ and the torque $\mathbf{T}_{contact,a}$. The heat transfer from the fluid to the particles is calculated by interpolation of the gas temperature (T_g) given at the Eulerian grid points surrounding the particle position. The temperature of every individual particle ($T_{p,a}$) with a constant heat source is given by the following heat balance equation:

$$\rho_p V_p C_{p,p} \frac{dT_{p,a}}{dt} = -hA_p \left(T_{p,a} - T_g\right) + \dot{q} V_p \quad (14)$$

Where $\dot{q}$ is the volumetric heat production rate due to the reaction and h is the particle interfacial heat transfer coefficient. The latter is calculated from the empirical correlation by Gunn (1978):

$$Nu_p = (7 - 10\varepsilon_g + 5\varepsilon_g^{\,2})(1 + 0.7\,\mathrm{Re}_p^{0.2}\,\mathrm{Pr}^{0.33}) + (1.33 - 2.40\varepsilon_g + 1.20\varepsilon_g^{\,2})\,\mathrm{Re}_p^{0.7}\,\mathrm{Pr}^{0.33} \quad (15)$$

$$Nu_p = \frac{h d_p}{k_g} \quad Pr = \frac{\mu_g C_{p,g}}{k_g}, \quad \mathrm{Re}_p = \frac{\varepsilon_g \rho_g \left|\mathbf{u}_g - \mathbf{v}_p\right| d_p}{\mu_g} \quad (16)$$

where Re_p and Pr are the particle Reynolds and Prandtl number, respectively.

SIMULATION SETTINGS

Fluidized bed geometry and particle properties

In all simulations a pseudo-2D fluidized bed was used to investigate the effect of elevated pressure on the fluidization behaviour. Details of the geometry, gas and particle properties are given in Table 1.

Initially, 8×10^4 polypropylene particles are randomly placed in the bed. At the bottom, gas is introduced with a uniform velocity, whereas at the top of the bed a pressure outlet with a constant pressure of respectively 1 bar, 2 bar, 5 bar, 10 bar or 20 bar is used for different simulation cases. No-slip boundary conditions are applied to the side-walls, whereas a free-slip boundary conditions are used for the front and back walls of the bed for solving the momentum equations for gas phase.

To enable a fair comparison, we compared cases with a constant excess superficial gas velocity ($u_{ex}=u_0-u_{mf}=0.285$ m/s), which is defined as the difference between the superficial velocity and the minimum fluidization velocity. The minimum velocities calculated from the Ergun equation (Ergun 1952) with solid volume fraction equal to 0.62 are 0.215, 0.165, 0.105, 0.085, 0.055 m/s for the different operating pressures.

RESULTS

Porosity distribution

All results discussed in this paper were analysed after both a hydrodynamic and thermal steady state were reached. Data was gathered during a period of 2 s with intervals of 0.0125 s. From the work of Godlieb et al. (2008) it was found that the solid mixing time in the fluidized bed with same size as this work was 1.5~2.0 s. In that work the same range of pressures was studied. Based on this, an analysis duration of 2 s is sufficient to characterize the solid behaviour of the whole bed. The probability distribution function (PDF) of the bed voidage was calculated on every Eulerian grids and the result is shown in Figure 1 for different operating pressures.

Table 1: Simulation properties.

Geometry		
Size of bed in x-direction	0.08	m
Size of bed in y-direction	0.01	m
Size of bed in z-direction	0.4	m
Particle number	8×10^4	-
Cell size	0.0025	m
Number of cells	30×4×160	-
Particle phase		
Density	667	kg/m^3
Specific heat capacity	1.67×10^3	J/(kg·K)
Particle diameter	0.995	mm
Normal coefficient of restitution (particle-particle)	0.60	N/m
Tangential coefficient of restitution (particle-particle)	0.33	N/m
Normal spring stiffness	1600	N/m
Tangential spring stiffness	800	N/m
Gas phase		
Molar mass	42.08	g/mole
Viscosity	1.0×10^{-5}	Pa s
Thermal conductivity	2.09×10^{-2}	J/ (m s K)
Specific heat capacity	1.67×10^3	J/(kg K)

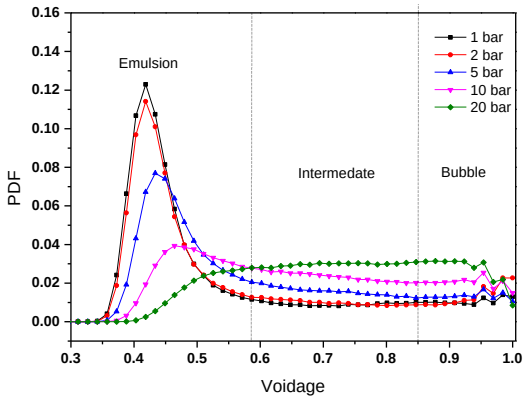

Figure 1: Probability distribution function (PDF) of the bed voidage as a function of operating pressure.

For pressures lower than 10 bar, we can observe a peak in the porosity range of 0.40 to 0.55, which was distinguished as emulsion phase. However, when the pressure is increased beyond 10 bar, this dominant peak disappears and most of the bed is in a state that is in between those of the dense emulsion phase and the bubble phase. With increasing pressure the bubble phase starts to contain more particles, whereas the emulsion phase contains more gas.

Similar observations were made by Godlieb et al. (2008). From animations of the simulations, it was observed that at these pressures due to extensive bubble breakup and

coalescence, the gas moves in the bed without typical bubble structure, which is observed at low pressures. The chaotic movement and increased interaction between particles and gas eliminates the distinct boundary between bubbles and the dense phase at high pressures. Smaller bubbles with lower rising speeds and higher break-up rate lead to tortuous bubble trajectories. These typical characteristics of fluidized beds at elevated pressure are in line with the findings of others (Li and Kuipers, 2002; Zhang, Li, and Fan, 2000).

Particle temperature distribution

Particle temperature PDF

In this section we will investigate the influence of the elevated pressure on the particle temperature distribution. To this end, the same set of superficial velocities and operating pressures as discussed before were used. This effect has been quantified by considering the probability distribution function (PDF) of the normalized particle temperature that is shown in Figure 2. In this figure, the driving force for heat transfer ($T_{p,a}$-$T_{g,0}$) has been normalized by dividing it by the difference between the melting point of polypropylene and the inlet gas temperature ($T_{p,m}$-$T_{g,0}$). The melting point of polypropylene is $T_{p,m}$ = 380 K. Figure 2 shows that at low pressure many particles get temperatures that are close to the melting point of polypropylene (high values of the temperature ratio). With increasing pressure, the particles get a more constant temperature and are further away from the melting point (the temperature ratio). Operating the bed at an elevated pressure is not only an essential condition for the polymerization process but it is also an efficient way to remove excessive polymerization reaction heat, and leads to a more homogeneous temperature distribution in the bed. In the inset in Figure 2 the standard deviation of the particle temperature is also shown, which is defined as:

$$\sigma = \sqrt{\frac{1}{N_p}\sum_{i=1}^{N_p}(T_{p,i} - \hat{T}_p)^2} \qquad (17)$$

The standard deviation also shows that the particle temperature is more uniformly distributed over the bed at increasing pressure. There may be several explanations for this behavior. One explanation is that increasing pressure leads to different bed dynamics, in particular leading to rapid solids mixing (Godlieb et al., 2008), which leads to quick replacement of the particles in the main pathway of the gas. Another explanation is that by increasing the pressure, the volumetric heat capacity of the gas is considerably increased, which gives the gas a much stronger capacity to cool the particles.

Instantaneous snapshots

Figure 3 shows the driving force for gas-particle heat transfer, which is characterized by the difference between the temperature of the individual particles ($T_{p,a}$) and the spatially averaged gas temperature ($<T_g>$). For the convenience of discussion, we also show the corresponding gas velocity magnitude vector fields underneath to indicate the main pathways of the gas moving through the bed. Note that the temperature scales for the driving force shown are different, i.e. the maximum value of the driving force is around 1 K in all cases. However, the minimum value changes considerably as a function of the operating pressure. Negative values of the driving force indicate particles with a temperature lower than the average bed temperature. These particles are primarily found near the bottom of the bed where they get in contact with the cold inlet gas. Some particles are dragged along with the gas moving along the main pathway of the gas, leading to the low temperature 'fingers'. These fingers can be used to trace how and where the gas is passing through the bed. With the corresponding instantaneous gas velocity vector graphs beneath the driving force distribution graphs (Figure 3 a2~e2), it clearly demonstrates that gas passes through the solids by moving from bubble to bubble. The cold particles (e.g. those with a strong negative driving force) are found between these bubbles. Besides the information obtained from the patterns and temperature differences, it is also noticeable that the differences in driving force are diminishing with increasing pressure, leading to a more isothermal bed.

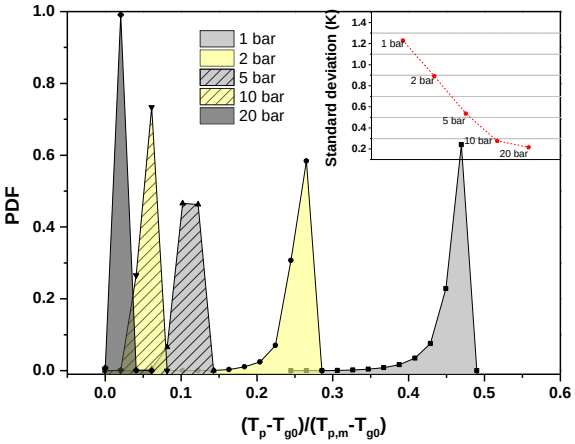

Figure 2: Particle temperature PDF and standard deviation when increasing operating pressure from 1 bar to 20 bar while keeping the same excess velocity (u_0-u_{mf}).

Particle Reynolds and Nusselt number distribution

In the previous section, the instantaneous snapshots of the particle temperatures have been used to discuss the effect of the operating pressure on the hydrodynamics and thermal behavior in a fluidized bed. However, the heat transfer coefficient has no direct relation to the particle temperature. To discuss the effect of the pressure on the heat transfer coefficient, instantaneous snapshots of Nu_p and Re_p are shown in Figure 4. Increasing the operating pressure leads to both higher values of Nu_p and Re_p, which can be observed clearly from the increasing scales alongside each graph of Figure 4. The instantaneous snapshots of Nu_p in graphs Figure 4-a1~e1) show that most particles with high and low Nu_p value are distributed in the wake of a bubble and in the bubble clouds, respectively. These differences cannot be explained from the corresponding distributions of Re_p, which are distributed such that low values of Re_p are found inside the bubbles, whereas high values of Re_p are found in the dense phase. The differing trends in Nu_p and Re_p indicate that apart from the differences in Re_p, local distribution of the volume fraction also determine the distribution of convective heat transfer coefficient.

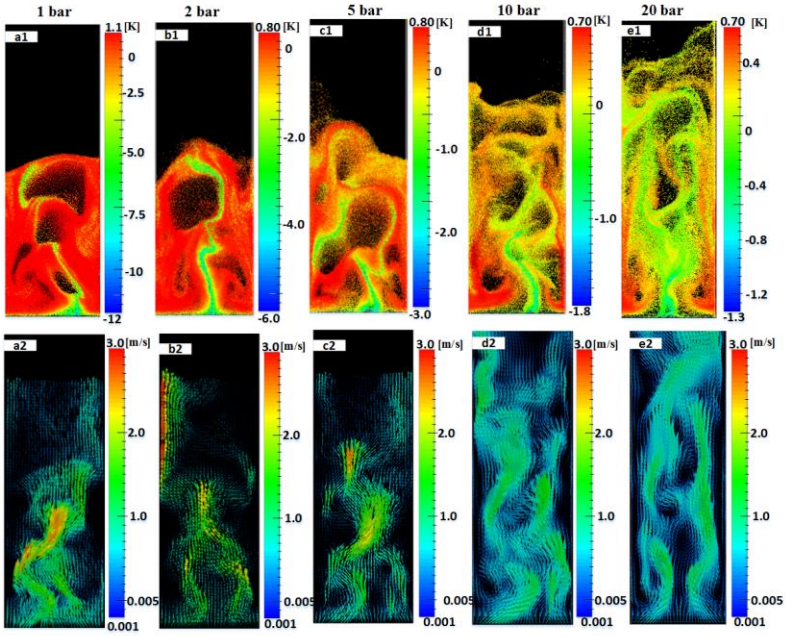

Figure 3: Snapshots of the driving force (T_p-<T_g>) plots with increasing operating pressure, and corresponding instantaneous gas velocity vector maps.

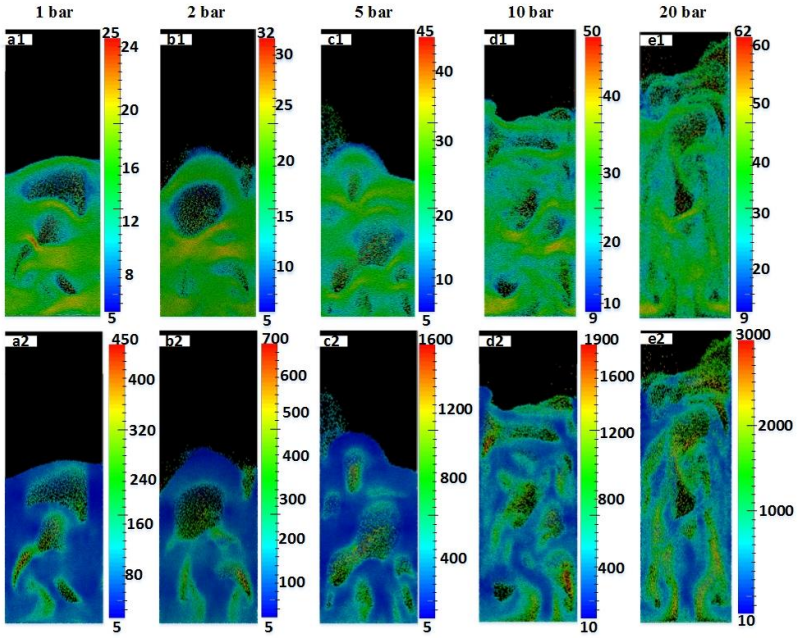

Figure 4: Snapshots of particle Nu_p (a1~e1) and Re_p (a2~e2) distribution patterns. Note that different color scales are used for reasons of clarity.

For practical purposes it is often desirable to a priori estimate the heat transfer coefficient. However, this depends on a characteristic particle Re_p and a characteristic voidage ε_g, both of which depend on the operating conditions. We can use our CFD-DEM simulation results to find out what definitions of Re_p and ε_g are best suited for this purpose. We have compared different heat transfer coefficients in terms of the Nu_p as a function of different definitions of Re_p and ε as shown in Figure 5. The differences of cases are from the simulations with different operation superficial velocities while keeping a constant excess superficial gas velocity for elevated pressure in each case. The simulation conditions and results of Nu_p from DPM are listed in the Appendix, where case 2 was used as example case discussed in the previous sections. In Figure 5 The black star symbols represent the time and spatially averaged Nusselt numbers from all the particles in a CFD-DEM simulation and are considered here as the 'true' Nu_p. The other symbols are calculated from equation 13 using different definitions of Re_p and ε_g. Re_{mf} is the particle Reynolds number at minimum fluidization condition, in which the gas velocity used is the minimum fluidization velocity u_{mf}, while Re_{u0} is the Re_p calculated by using the superficial velocity u_0. ε_{mf} and ε_{DPM} are the porosity at minimum fluidization (0.38) and the spatially averaged porosity calculated from the CFD-DEM simulations. The comparison suggests that to predict the heat transfer coefficient of a pressurized fluidized bed, using Re_{mf} and ε_{mf} can well predict the value of Nu_p. Meanwhile Nu_p can also be calculated by using Re_{u0}, whereas the porosity should be obtained from either a CFD-DEM simulation or from a bed expansion experiment.

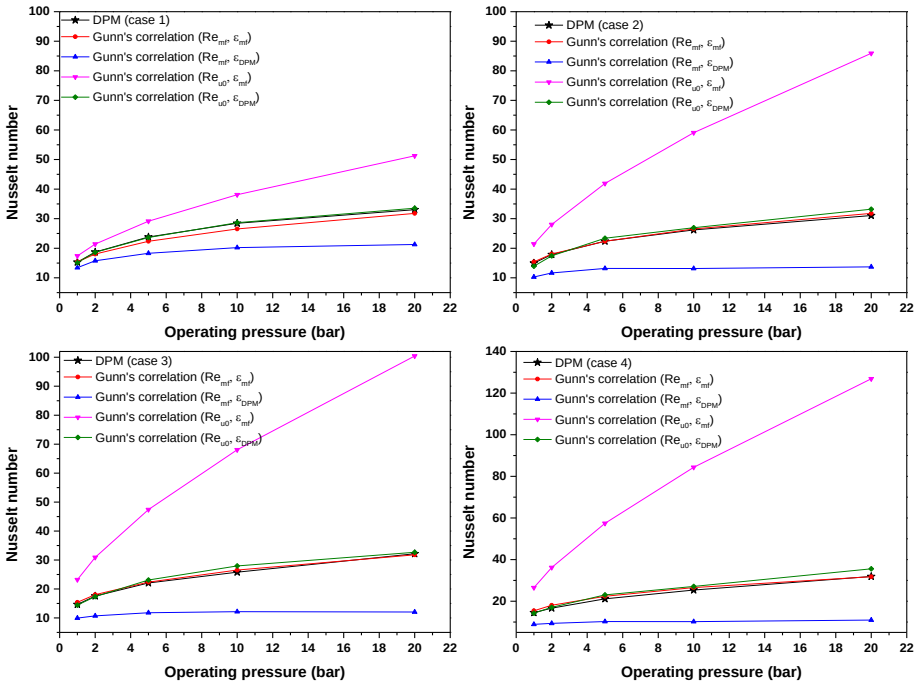

Figure 5: Time average Nu_p as a function of operating pressure obtained from CFD-DEM simulation and estimation data from Gunn's correlation.

CONCLUSION

In this work, a CFD-DEM model was used to simulate a gas phase polyolefin fluidized bed with a constant volumetric heat production in the particle phase. By increasing the operating pressure from 1 bar to 20 bar, with the same excess superficial velocity, it is found that the elevated pressure influences the hydrodynamics and significantly enhances the heat transfer performance of a fluidized bed. The bubble size is reduced and a flatter distribution of bed voidage is achieved. The PDF of the normalized particle temperature shows that the mean value decreases significantly, while the standard deviation decreases as the pressure is increased. Operating the bed at an elevated pressure helps to reach a more isothermal condition in the fluidized bed, thereby reducing the opportunity for hot spots to develop.

The convective heat transfer coefficient, which was characterized by the particle Nusselt number increases considerably with increasing operating pressure, which is beneficial for removing more heat from the bed. This can be entirely attributed to the increased density, whereas the changes in the bed hydrodynamics have little effect. To predict the heat transfer coefficient for a pressurized fluidized bed with Gunn's empirical correlation, it is suggested to use the particle Reynolds number calculated on basis of the gas velocity and bed porosity under minimum fluidization condition or Reynolds number from operation superficial velocity and the bed averaged porosity obtained from either CFD-DEM simulations or bed expansion experiments, in which the bed expansion as a function of the operating pressure also has to be considered.

ACKNOWLEDGEMENT

This research is part of research programs of Dutch Polymer Institute (DPI) as project #751.

REFERENCES

CHOI, K.Y. and RAY, W.H., (1985). "Polymerization of olefins through heterogeneous catalysis. II. Kinetics of gas phase propylene polymerization with Ziegler–Natta catalysts", *J. Appl. Polym. Sci*, **30**, 1065–1081.

ERGUN, S., (1952), "Fluid flow through packed columns". *Chem. Eng. Prog.*, **48**, 89–94.

GODLIEB, W., DEEN, N.G. and KUIPERS, J.A.M., (2008), "On the relationship between operating pressure and granular temperature: A discrete particle simulation study", *Powder Technol.*, **182,** 250–256.

GUNN, D.J., (1978), "Transfer of heat or mass to particles in fixed and fluidised beds", *Int. J. Heat Mass Transfer*, **21**, 467–476.

LI, J. and KUIPERS, J.A.M., (2002), "Effect of pressure on gas–solid flow behaviour in dense gas-fluidized beds: a discrete particle simulation study", *Powder Technol.*, **127**, 173–184.

SIDORENKO, I. and RHODES, M.J., (2004). "Influence of pressure on fluidization properties", *Powder Technol*, **141**, 137–154.

YATES, J. and SIMONS, S., (1994). "Experimental Methods in Fluidization Research", *Int. J. Multiphase Flow*, **20**, 297–330.

WEN, C.Y. and YU, Y.H., (1966), " Mechanism of fluid", *Chem. Eng. Prog. Symp.*, **62**, *pp 100-110.*

ZHANG, J., LI, Y. and FAN, L.S., (2000), "Numerical studies of bubble and particle dynamics in a three-phase fluidized bed at elevated pressures", *Powder Technology*, **112**, 46–56.

APPENDIX

Table A.1. List of simulation conditions and results of Figure 5

Case 1						
p (bar)	u_0 (m/s)	u_{mf} (m/s)	u_{exc}(m/s)	ε_{DPM}	Re_{DPM}	Nu_{DPM}
1	0.30	0.215	0.085	0.58	77.11	15.30
2	0.25	0.165	0.085	0.45	76.83	18.70
5	0.19	0.105	0.085	0.47	150.65	23.81
10	0.17	0.085	0.085	0.50	255.27	28.46
20	0.14	0.055	0.085	0.56	439.99	33.05
Case 2						
p (bar)	u_0 (m/s)	u_{mf} (m/s)	u_{exc}(m/s)	ε_{DPM}	Re_{DPM}	Nu_{DPM}
1	0.50	0.215	0.285	0.58	59.20	14.97
2	0.45	0.165	0.285	0.59	100.68	17.87
5	0.40	0.105	0.285	0.62	207.34	22.39
10	0.37	0.085	0.285	0.70	371.21	26.19
20	0.34	0.055	0.285	0.75	674.71	31.06
Case 3						
p (bar)	u_0 (m/s)	u_{mf} (m/s)	u_{exc}(m/s)	ε_{DPM}	Re_{DPM}	Nu_{DPM}
1	0.60	0.215	0.385	0.60	63.17	14.67
2	0.55	0.165	0.385	0.63	115.41	17.55
5	0.49	0.105	0.385	0.68	228.47	22.08
10	0.47	0.085	0.385	0.73	419.61	25.79
20	0.44	0.055	0.385	0.82	807.71	32.16
Case 4						
p (bar)	u_0 (m/s)	u_{mf} (m/s)	u_{exc}(m/s)	ε_{DPM}	Re_{DPM}	Nu_{DPM}
1	0.80	0.215	0.585	0.66	79.69	14.47
2	0.75	0.165	0.585	0.70	139.76	16.67
5	0.69	0.105	0.585	0.75	287.20	21.15
10	0.67	0.085	0.585	0.83	609.70	25.37
20	0.64	0.055	0.585	0.89	1112.00	31.88